International Journal of Heat and Mass Transfer 54 (2011) 4730–4735

Contents lists available at ScienceDirect

International Journal of Heat and Mass Transfer

journal homepage: www.elsevier.com/locate/ijhmt

Nonlinear temperature field near the stack ends of a standing-wave thermoacoustic refrigerator

Arganthaël Berson [a,*], Gaëlle Poignand [b], Philippe Blanc-Benon [c], Geneviève Comte-Bellot [c]

[a] Department of Chemistry, University of Durham, South Road, Durham DH1 3LE, United Kingdom
[b] Laboratoire d'Acoustique de l'Université du Main, UMR CNRS 6613, Avenue Olivier Messiaen, 72085 Le Mans Cedex 9, France
[c] Laboratoire de Mécanique des Fluides et d'Acoustique, UMR CNRS 5509, École Centrale de Lyon, 36 avenue Guy de Collongue, 69134 Ecully-Cedex, France

ARTICLE INFO

Article history:
Received 4 January 2011
Received in revised form 27 May 2011
Available online 28 June 2011

Keywords:
Thermoacoustics
Temperature-fluctuation measurements
Constant-voltage anemometry
Oscillating flows

ABSTRACT

The nonlinear temperature field in the vicinity of the stack of a standing-wave thermoacoustic refrigerator is investigated both theoretically and experimentally. First, the problem is addressed theoretically by a one-dimensional nonlinear model that predicts the generation of thermal harmonics near the ends of the stack. The model relies on a relaxation-time approximation to describe transverse heat transfer between the stack walls and the working fluid. It extends a previous model proposed by [Gusev et al., Thermal wave harmonics generation in the hydrodynamical heat transport in thermoacoustics, J. Acoust. Soc. Am. 109 (2001) pp. 84–90], by including the effect of axial conduction on temperature fluctuations. Second, the nonlinear temperature field is investigated experimentally. The amplitude of temperature fluctuations behind the stack at the fundamental frequency and second harmonic are measured using cold-wire anemometry. The measurements rely on a procedure recently developed by the authors that allows a full correction of the thermal inertia of the sensor. Experimental results are in good agreement with the predictions of the model. The generation of thermal harmonics behind the stack is thus validated. The influence of the Péclet number on the thermal field, which depends on the diffusivity of the working fluid and on the acoustic frequency and pressure level, is also demonstrated.

1. Introduction

Thermoacoustic systems convert thermal energy into acoustic energy and vice versa. In thermoacoustic refrigerators, the interaction between a high-amplitude acoustic wave and a porous medium (usually referred to as "stack") creates a heat flux along the porous medium. Thermoacoustic refrigerators have a simple architecture with no moving parts save for the driver, which makes them robust and reliable, and opens possibilities for low cost production and miniaturization. In addition, they operate with working fluids such as binary mixtures of noble gases that are benign to the environment. In order to enhance the performances of these systems, it is necessary to improve the efficiency of each of their components as well as of the coupling between these components.

The coupling between the stack and the heat-exchangers is often modelled using a mean-field approximation as in Refs. [18] or [13] for instance. Models relying on this approximation neglect the contribution of longitudinal gradients of temperature oscillations to the convective heat flux along the stack. However, when longitudinal gradients of temperature oscillations are not neglected, analytical models by Gusev et al. [9,10] and numerical models by Karpov and Prosperetti [12] showed that, near the ends of a thermoacoustic stack, the thermal field is nonlinear. This was further validated by direct numerical simulations [7,14,15]. In fact, thermal harmonics are generated near the ends of the stack that affect the transport of heat towards/from the heat-exchangers. Contrary to the results of the linear theory, which predicts that the stack and heat-exchangers should be adjacent [22], nonlinear models predict that the enthalpy flux between the stack and the heat exchanger is maximised when an optimal gap is introduced between the two components. Therefore, the first objective of the present study is to improve the theoretical understanding of the nonlinear temperature field near the stack ends.

Matveev et al. [16,17] recently published mean temperature measurements behind the thermal buffer tube of some thermoacoustic systems. They successfully compared their measurements to a semi-analytical model that has some similarities with the one described in Refs. [9,10]. However, to date, there is no experimental evidence of the generation of thermal harmonics near the stack ends. Cold-wire measurements of the temperature oscillations were performed inside the boundary layer along a stack plate by Huelsz and Ramos [11], but the data were acquired far from the

* Corresponding author.
E-mail address: arganthael.berson@durham.ac.uk (A. Berson).

0017-9310/$ - see front matter © 2011 Elsevier Ltd. All rights reserved.
doi:10.1016/j.ijheatmasstransfer.2011.06.003

Nomenclature

BR	blockage ratio
c_p	specific heat of the fluid
c_w	specific heat of the wire material
d_{ac}	acoustic displacement
D	diffusivity of the fluid
$f(U)$	a function of the velocity describing convective heat transfer
f_{osc}	fundamental frequency of acoustic oscillations
h	convective heat transfer coefficient
k_f	conductivity of the fluid
m_w	mass of the wire
$\mathcal{M}_{CCA}$	time lag of the cold wire
P'	acoustic pressure fluctuations
$\widehat{P}'$	average of P' over the cross section
P_{ac}	amplitude of acoustic pressure fluctuations
P_m	mean pressure of the fluid
Pe^{-1}	inverse of the Péclet number
R	dimensionless relaxation coefficient
R_{CCA}	resistance of the real wire
R^*_{CCA}	resistance of the ideal wire
R_0	resistance of the wire at a reference temperature T_0
r_L	resistance of the connection cable
S	surface area of a channel cross section
t	time
T_a	temperature of the fluid
T_0	reference temperature
T_m	mean temperature of the fluid
T'	temperature fluctuations of the fluid
T'_s	temperature fluctuations of the channel walls
$\widehat{T}'$	average of T' over the cross section
U	velocity component normal to the wire
u'	velocity fluctuations
V_w	voltage across the wire
x	axial coordinate, origin at the hot end of the stack
y, z	transverse spatial coordinates
β	isobaric thermal expansion coefficient of the fluid
$\Delta\xi$	dimensionless space interval
$\Delta\tau$	dimensionless time interval
θ	dimensionless temperature fluctuations
θ_1	dimensionless amplitude of temperature fluctuations at f_{osc}
θ_2	dimensionless amplitude of temperature fluctuations at $2f_{osc}$
ξ	dimensionless position
Π	perimeter of a channel cross section
ρ_f	fluid density
τ	dimensionless time
τ_R	relaxation time
χ	temperature coefficient of resistivity for the wire material
ω	angular frequency

stack ends and they were limited to the fundamental frequency. The oscillating temperature field inside the stack channels and near the stack ends were measured using holographic interferometry [23] and more recently using laser-induced fluorescence [21]. These results show that the temperature field is disturbed near the stack ends, in part due to the generation of vorticity when the stack plates are thick [23]. However, these experiments are not representative of real thermoacoustic systems since the temperature gradient is imposed by heaters located along a single plate in one case [23] and the stack is replaced by two adjacent heat-exchangers in the other [21]. In this context, the second objective of the present study is to make up for the lack of measurements of temperature fluctuations in realistic thermoacoustic devices.

The present paper is organized as follows: Section 2 presents a one-dimensional nonlinear model that describes the acoustic temperature field behind the stack. The model is an extension of the work by Gusev et al. [9,10], to which the contribution of axial conduction was added. Indeed, we shall see that axial conduction has a significant effect on the results. Section 3 describes the experimental setup and it introduces the novel procedure that we developed recently for the measurements of temperature fluctuations in oscillating flows using cold wires [5]. The procedure relies on the unique features of constant-voltage anemometers (CVA) to correct the thermal inertia of cold wires. Following this procedure, accurate measurements of the temperature fluctuations behind the stack are performed. Experimental results are presented in Section 4 and compared with the model predictions.

2. Theoretical model

The model is an extension of the one proposed by Gusev et al. [9,10]. For a thermoacoustic standing-wave refrigerator, the temperature fluctuations inside the channels of the stack are given by the following equation:

$$\frac{\partial T'}{\partial t}+u'\frac{\partial T'}{\partial x}=\frac{\beta T_m}{\rho_f c_p}\left(\frac{\partial P'}{\partial t}+u'\frac{\partial P'}{\partial x}\right)+D\left(\frac{\partial^2 T'}{\partial x^2}+\frac{\partial^2 T'}{\partial y^2}+\frac{\partial^2 T'}{\partial z^2}\right), \tag{1}$$

where the different notations are given in the nomenclature and the isobaric thermal expansion coefficient of the fluid is $\beta = \rho_f c_p(\gamma-1)/(\gamma P_m)$. Similarly to Gusev et al. [9,10], the effect of viscous stress on the temperature field is neglected in Eq. (1). The flow is one-dimensional, i.e. velocity depends on x and t only, so that the model does not account for viscous boundary layers along the plates nor for vortices that may appear behind the stack edges. The thermophysical properties of the fluid and solid are assumed to be constant. However, contrary to Gusev et al. [10], the term $D\partial^2 T'/\partial x^2$, which describes the conductive heat transfer in the axial direction, is not neglected in our model.

As already noted by Gusev et al. [10], the second term of the right-hand side of Eq. (1) is small compared to the first term and velocity fluctuations do not depend on the y and z directions. Temperature fluctuations T' can therefore be averaged over the channel cross section S and this quantity is denoted $\widehat{T}'$. In addition, transverse heat transfer averaged over the channel cross section is modeled using Newton's law of cooling by [10]

$$D\int\int_S\left(\frac{\partial^2 T'}{\partial y^2}+\frac{\partial^2 T'}{\partial z^2}\right)dS = D\oint_\Pi \frac{h}{k_f}(T'_s-\widehat{T}')d\Pi, \tag{2}$$

where S and Π are the surface area and perimeter of a channel cross section, respectively. h is the convective heat transfer coefficient and k_f is the conductivity of the fluid. T'_s are the temperature fluctuations of the channel walls, which are neglected. The relaxation time τ_R can be introduced

$$\tau_R=\frac{Sk_f}{\Pi D h}, \tag{3}$$

and Eq. (1) is re-written as

$$\frac{\partial \widehat{T}'}{\partial t} + u' \frac{\partial \widehat{T}'}{\partial x} = \frac{\beta T_m}{\rho_f c_p} \frac{\partial \widehat{P}'}{\partial t} - \frac{\widehat{T}'}{\tau_R} + D \frac{\partial^2 \widehat{T}'}{\partial x^2}. \tag{4}$$

The following dimensionless variables are introduced:

$$\theta = \frac{\widehat{T}'}{T'_{ad,0}}, \tag{5}$$

$$\xi = \frac{x}{d_{ac}}, \tag{6}$$

$$\tau = \omega t, \tag{7}$$

$$R = \omega \tau_R, \tag{8}$$

$$Pe^{-1} = \frac{D}{\omega d_{ac}^2}, \tag{9}$$

where θ represents the temperature fluctuations normalized by the amplitude of adiabatic temperature fluctuations $T'_{ad,0}$ due to the acoustic wave only, ξ is the distance normalized by the acoustic displacement d_{ac}, τ is the time normalized by the fundamental acoustic angular frequency, R is the dimensionless relaxation time, and Pe^{-1} is the inverse of the Péclet number based on the acoustic displacement d_{ac} and the magnitude of the acoustic velocity $u'_0 = \omega d_{ac}$. Finally, Eq. (4) is re-written in a dimensionless form as

$$\frac{\partial \theta}{\partial \tau} + \sin\tau \frac{\partial \theta}{\partial \xi} = \sin\tau - \frac{\theta}{R} + Pe^{-1} \frac{\partial^2 \theta}{\partial \xi^2}. \tag{10}$$

Eq. (10) is the governing equation to solve in order to describe the nonlinear thermal field in the channels of the stack and near its ends. Before going further, we draw the attention on a major assumption made in this model. As discussed previously by Gusev et al. [10], the calculation of the dimensionless relaxation time R would require the solution of the transverse heat transfer problem along the stack. Instead, in the present model, the relaxation time is considered as a phenomenological parameter used to close the governing equation. This assumption greatly simplifies the model. Moreover, as the experiments will show later, the model provides a good qualitative description of the oscillating temperature field and agrees very satisfactorily with the experiments.

Because of the addition of the axial-conduction term in Eq. (10), this equation can no longer be solved analytically as in Refs. [9,10]. Therefore, Eq. (10) is solved numerically using a finite-difference scheme in both time and space. The computational domain ranges from $\xi = -4$ to $\xi = 11$ in space and covers 75 acoustic periods in time. Time and space intervals are $\Delta\tau = 0.05$ and $\Delta\xi = 0.05$ respectively. We verified that the solutions are converged and that the system has reached a stationary state.

The stack is located at $\xi \leqslant 0$. At locations $\xi > 0$, the fluid is only subject to the acoustic wave and does not exchange temperature with its surroundings. The regime is adiabatic and we set $R = 10000 \approx \infty$. This can be seen in Fig. 1, which describes the position and the temperature of three fluid particles at different locations in the domain during an acoustic period. The rightmost particle never enters the stack and undergoes adiabatic temperature oscillations throughout the acoustic cycle, which corresponds to a straight line on the figure.

In the stack domain, we set $R = 1$, which is the optimal regime for thermoacoustic transport [10]. The optimal regime stands between the adiabatic regime and the isothermal one ($R \to 0$). A particle of fluid travelling inside the stack exchanges heat with the channel walls and forms an ellipse in Fig. 1 (leftmost particle).

The most interesting case is when fluid particles cross the boundary between the stack and the adiabatic region. The middle particle in Fig. 1 undergoes an adiabatic regime during one half of the acoustic cycle and the optimal thermoacoustic regime during the rest of the acoustic cycle. This change in transverse heat-transfer regime experienced by the fluid particles near the edge of the stack is responsible for the generation of thermal harmonics [9,10], as can be seen in Fig. 2.

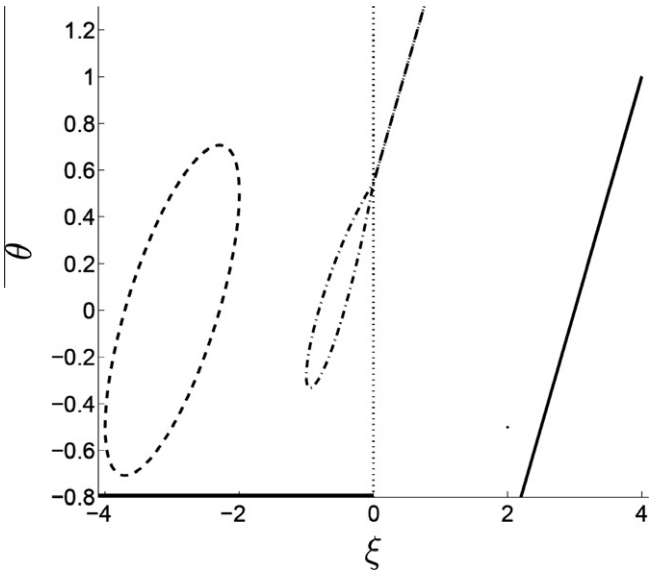

Fig. 1. Position and temperature of three fluid particles during an acoustic cycle. The leftmost particle spends the entire acoustic cycle inside the stack ($R = 1$ at $\xi \leqslant 0$). The rightmost particle spends the entire acoustic cycle outside the stack ($R = \infty$ at $\xi > 0$). The middle particle crosses the edge of the stack. Axial conduction is neglected, $Pe^{-1} = 0$.

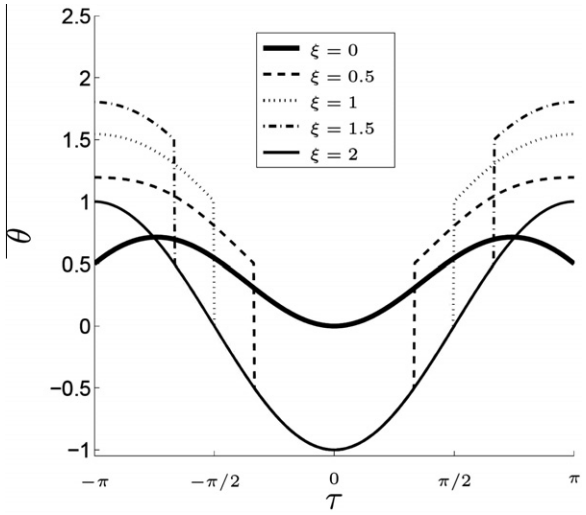

Fig. 2. Temperature fluctuations predicted by the model during an acoustic period at different locations near the stack end. $R = 1$ inside the stack, $R = \infty$ outside the stack, $Pe^{-1} = 0$.

Fig. 2 shows the time evolution of temperature fluctuations at different locations close to the hot end of the stack. Within a region expanding $\xi = 2$ away from the end of the stack, temperature oscillations are distorted. The distortion of the thermal field, previously observed in numerical computations [14,15], is expected to affect heat transport between the stack and the heat-exchangers. Indeed, analytical calculations based on a model similar to the one presented here [3,9] as well as numerical simulations [7,14,15] have shown that, because of the nonlinearity of the thermal field, there exists an optimal gap between the stack and the heat-exchangers that maximises heat transport.

3. Experimental setup

3.1. Thermoacoustic refrigerator and instrumentation

The thermoacoustic refrigerator is similar to the one used in Ref. [1] and it is sketched in Fig. 3. The system consists of a quarter-wavelength standing-wave acoustic resonator, a stack of plates and sensors. The resonator is a 15-cm long straight cylindrical tube of diameter 3 cm. A 3-cm long exponential horn connects one end of the tube to the electrodynamic driver (GELEC EDM8760F). The other end is closed. The driver generates acoustic pressure levels up to 3000 Pa at the fundamental frequency of f_{osc} = 465 Hz in air at ambient temperature and atmospheric pressure. The acoustic pressure is monitored by a 1/4 inch Brüel & Kjær microphone located 90 mm away from the closed end of the resonator.

The stack is made of parallel glass plates of thickness 0.17 mm of length 18 mm and separated by 0.41 mm. The total blockage ratio of the stack, including the support is BR = 0.37. The hot side of the stack is located 37 mm away from the closed end of the resonator. In this configuration, a mean temperature gradient of approximately 9 K develops along the stack at P_{ac} = 3000 Pa. All the temperature fluctuations presented here are deviations from the local mean temperature at the hot side of the stack.

Temperature measurements are performed with a small tungsten wire. The diameter of the wire is approximately 3 μm and its length is 3 mm. The wire is mounted on a L-shaped probe (Dantec 55P04). It is very important that the wire be mounted on such a L-shaped probe in order to avoid thermoacoustic interactions between the fluid and the wire support during an acoustic cycle [2]. The reference resistance of the wire is R_0 = 24.9 Ω at the reference temperature T_0 = 293 K and the resistance of the connection cable is r_L = 0.7 Ω. The wire is inserted in the resonator through a rubber membrane embedded in the end wall, which ensures an adequate sealing. The distance between the wire and the stack plates along the resonator axis is controlled with an accurate linear stage and monitored with a camera equipped with a zoom lens. The wire is set parallel to the stack plates and in front of the shear layers developing along the plate surface.

3.2. Procedure for temperature measurements in oscillating flows using cold wires

The measurements of temperature fluctuations behind the stack follow the procedure that was previously developed and validated in [5]. To our knowledge, this is the only procedure available that allows the accurate measurements of temperature fluctuations in oscillating flows using cold wires, despite their thermal inertia [6]. In the following, this procedure is briefly summarized. More details can be found in [5].

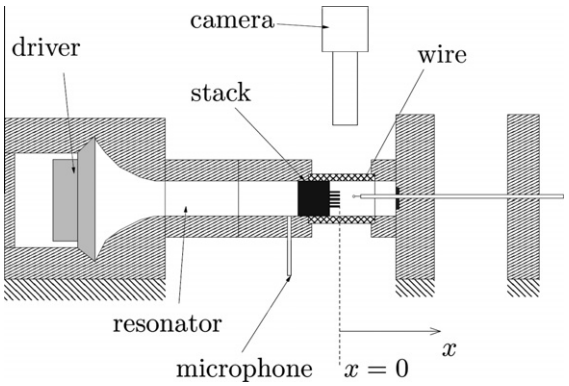

Fig. 3. Experimental setup.

When operated in the constant-current mode (CCA) with a very low overheat, the resistance $R^*_{CCA}(t)$ of an ideal wire varies with the temperature of the surrounding fluid:

$$T_a(t) - T_0 = \frac{R^*_{CCA}(t) - R_0}{R_0 \chi}. \tag{11}$$

The wire is ideal because it does not undergo thermal inertia, contrary to a real wire that does not respond instantaneously to a change in the fluid temperature because of its mass and heat capacity. The resistance $R_{CCA}(t)$ of the real wire is related to the resistance of the ideal wire by the following equation

$$\mathcal{M}_{CCA}(t)\frac{dR_{CCA}(t)}{dt} + R_{CCA}(t) = R^*_{CCA}(t), \tag{12}$$

where $\mathcal{M}_{CCA}(t)$ is the time lag of the cold wire, which is given by:

$$\mathcal{M}_{CCA}(t) = \frac{m_w c_w}{\chi R_0}\frac{1}{f[U(t)]}. \tag{13}$$

$\mathcal{M}_{CCA}(t)$ can be separated into two terms. The first one $m_w c_w/\chi R_0$ depends on the wire properties and the second one is a function of the flow velocity $1/f[U(t)]$.

The first term of the time lag, $m_w c_w/\chi R_0$, is obtained by using the same wire operated in the heated mode by a CVA from Tao Systems Inc. [19,20], without the acoustic flow. Simple electrical measurements performed with the square-wave test module embedded in the CVA units yield the time constant of the wire, from which the coefficient $m_w c_w/\chi R_0$ is deduced. Note that the procedure does not require the knowledge of the thermophysical and geometrical properties of the wire, which is very convenient since, for instance, the wire diameter always differs from the specifications of the manufacturer.

The second term of the time lag, $1/f[U(t)]$, depends on the flow velocity and, hence, it is time dependent. In flows with large-amplitude velocity fluctuations, e.g. oscillating flows, it is necessary to use the instantaneous value of $\mathcal{M}_{CCA}(t)$ for the correction of the thermal inertia otherwise the measured temperature signal is distorted [8]. The measurement of $1/f[U(t)]$ is performed in situ, with the same wire operated in the heated mode but this time using the velocity module of a CVA. The hot wire is sensitive to the amount of heat conveyed away by the fluid flow so that the function $f[U(t)]$ is directly related to the voltage output of the CVA [4,5]. It is not necessary to know the fluid velocity itself. In other words, the procedure does not require any calibration in velocity. In addition, it corrects all the nonlinearities of the CVA in the hot-wire mode.

We perform measurements in the cold-wire and hot-wire modes alternately, the measurements being synchronized with the output signal of the monitoring microphone.

Cold-wire measurements are performed with the temperature module of a Dantec Streamline 90C20 anemometer. The intensity of the current flowing through the wire is maintained constant by the anemometer to I_{CCA} = 0.1 mA. Hot-wire measurements are performed with a CVA, model VC01 from Tao Systems, maintaining a constant voltage V_w = 910 mV across the wire. More details about the electronics and the parameters of the anemometers are given in [5].

During post-processing, Eq. (12) is solved numerically using $\mathcal{M}_{CCA}(t)$ that is deduced from CVA measurements, and the instantaneous temperature of the fluid is computed from the resistance of the ideal wire using Eq. (11) or a calibration curve. The parameter χ is determined in an auxiliary heated facility.

4. Results and discussions

Experimental results are compared to the predictions of the model in Figs. 4 and 5. Figs. 4 and 5 show the spatial distributions of the amplitudes θ_1 and θ_2 of temperature fluctuations behind the hot end of the stack at the fundamental frequency and twice the fundamental frequency, respectively. Measurements were performed at three different acoustic pressure levels: $P_{ac} = 1000$, 2000 and 3000 Pa. At these acoustic pressure levels, the amplitude of adiabatic temperature fluctuations induced by the acoustic wave are $T'_{ad,0} = 0.8$, 1.6 and 2.5 K respectively; the acoustic displacements are $d_{ac} = 0.7$, 1.4 and 2.0 mm respectively; and the inverse Péclet numbers are $Pe^{-1} = 16.3 \times 10^{-3}$, 3.8×10^{-3} and 1.9×10^{-3} respectively. The coefficients Pe^{-1} were calculated using $D = 2.2 \times 10^{-5} \mathrm{m}^2 \cdot \mathrm{s}^{-1}$ as the diffusivity coefficient of air. The results obtained with the analytical model by Gusev et al. [10], which corresponds to the case $Pe^{-1} = 0$ (no conduction), are also plotted. Note that, in order to account for the higher velocity amplitude

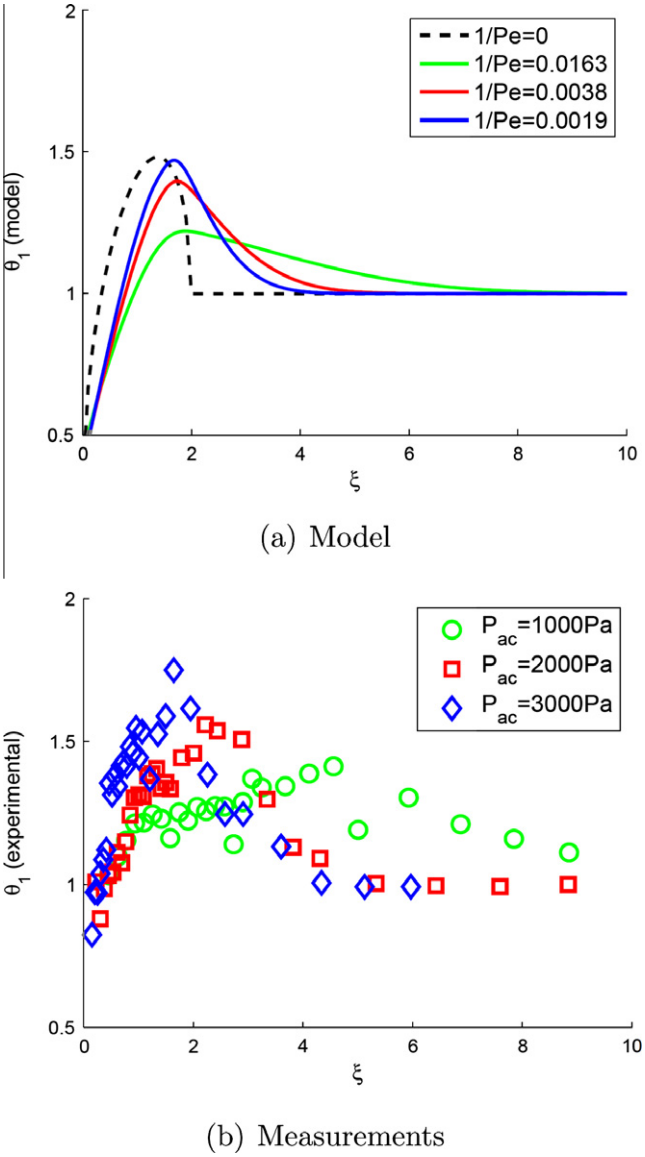

Fig. 4. Amplitudes of temperature fluctuations behind the stack at the fundamental frequency. Top: models. Bottom: measurements. Relaxation parameters used in the model: $R = 1$ inside the stack, $R = 10{,}000$ outside the stack. The hot end of the stack is located at $\xi = 0$.

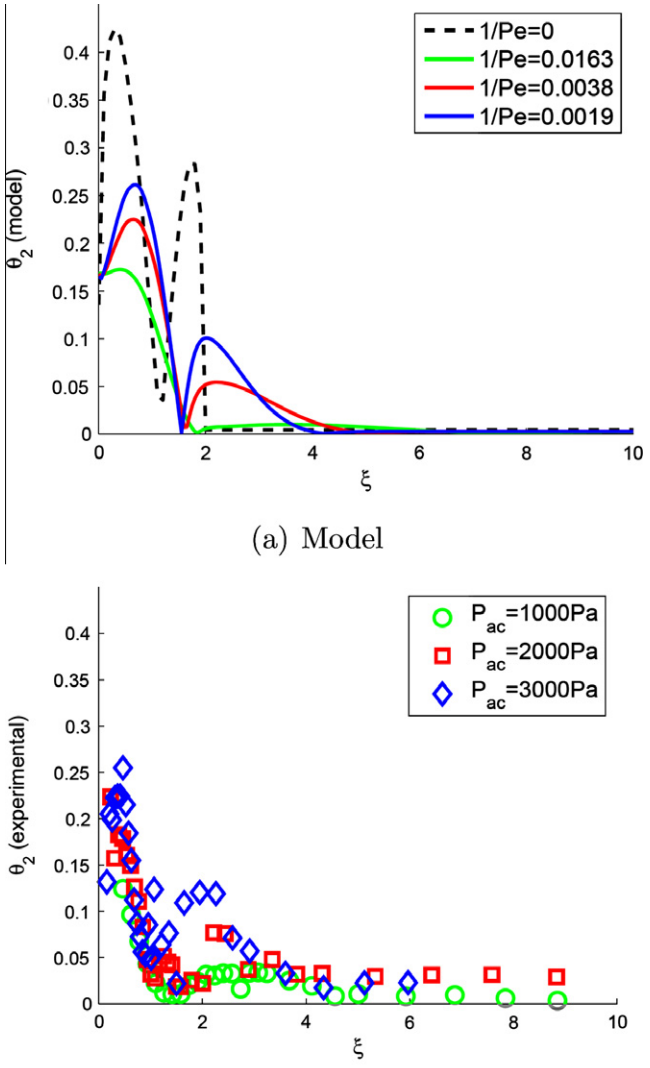

Fig. 5. Amplitudes of temperature fluctuations behind the stack at twice the fundamental frequency. Top: models. Bottom: measurements. Relaxation parameters used in the model: $R = 1$ inside the stack, $R = 10000$ outside the stack. The hot end of the stack is located at $\xi = 0$.

at the exit of the stack due to blockage, the blockage ratio is taken into account in the normalised acoustic displacement. In other words, in the following, $\xi = BR \times x/d_{ac}$.

First, the results from the model are examined in order to assess the effect of axial conduction on the thermal field behind the stack. As we saw previously, harmonics are generated due to the change in transverse-heat-transfer regime between the two regions of the domain. The analytical model, in which axial conduction is neglected, predicts that the thermal field is nonlinear up to $\xi = 2$ away from the stack edge. Indeed, a fluid particle driven by the acoustic wave oscillates with an amplitude of $2d_{ac}$ and the fluid particles in the region where $\xi > 2$ never interact with the stack. Adding axial conduction to the model extends the size of the perturbated region behind the stack beyond $\xi = 2$. The greater the inverse Péclet number Pe^{-1}, the further the perturbated region extends.

The analytical model, in the limit $Pe^{-1} = 0$, shows that θ_1 reaches a maximum at about $\xi = 1.4$ before going down to adiabatic temperature fluctuations $\theta_1 = 1$ at $\xi = 2$ (Fig. 4, top). Axial conduction

shifts the position of the maximum away from the stack and, as already mentioned, extends the zone where $\theta_1 > 1$ beyond $\xi = 2$. The maximum also decreases as Pe^{-1} increases, which flattens the spatial distribution.

The effect of axial conduction on θ_2 is similar. According to the analytical model, there are two maxima of θ_2 behind the stack located at approximately $\xi = 0.3$ and $\xi = 1.7$ (Fig. 5, top). The first peak is larger than the second one. Again, axial conduction shifts the perturbation away from the stack and beyond $\xi = 2$. Increasing Pe^{-1} decreases the amplitude of both peaks, the second one being more affected. For $Pe^{-1} = 0.0163$, the second peak is hardly distinguishable.

There is a good qualitative agreement between the model and the experiments. The results of the model presented in Fig. 4 (top) show the same trend as the experiments, Fig. 4 (bottom), i.e. a maximum of amplitude is observed, which decreases and is shifted away from the stack when the acoustic pressure decreases. Far from the stack, temperature fluctuations are no longer perturbated and follow an adiabatic cycle ($\theta_1 = 1$). For the amplitudes of the second harmonic, Fig. 5 (top) demonstrates that the trends predicted by the model compare satisfactorily with the measurements (Fig. 5, bottom). As the acoustic pressure decreases, i.e. axial conduction becomes more important, the two peaks decrease, the second one being more affected than the first one and extending beyond $\xi = 2$.

These experimental results validate the generation of temperature harmonics in the vicinity of the stack of a thermoacoustic refrigerator. In the present experiments conducted in air, the inverse of the Péclet number Pe^{-1}, which accounts for the effect of diffusion with respect to the convection provided by the acoustic wave, ranges between 0.0019 and 0.0163. These low values of Pe^{-1} suggest that diffusion is marginal compared to convection by the acoustic wave, which could justify that it was neglected in the initial model of Gusev et al. [9,10]. However, the present experimental results confirm the importance of axial conduction on the oscillating temperature field. Axial conduction tends to extend the region affected by nonlinearities but it also dampens the magnitude of temperature harmonics. Pe^{-1} depends on the acoustic displacement as well as on the diffusivity of the working fluid.

5. Conclusion

Thermal harmonics are generated near the ends of the stack of a thermoacoustic refrigerator. These harmonics are predicted by a nonlinear one-dimensional model relying on a relaxation time approximation to describe transverse heat transfer between the working fluid and the channel walls. The predictions of the model are validated successfully by measurements of the temperature fluctuations behind the stack. The measurements are made possible by a recently developed procedure for cold-wire thermometry that relies on the unique features of the CVA to correct the thermal inertia of the wire. We also show that the spatial distribution of the amplitude of temperature oscillations at the fundamental frequency and second harmonic near the stack are influenced by the Péclet number, which depends on the diffusivity of the working fluid and on the level and frequency of the acoustic wave. When the inverse of the Péclet number is large, the thermal harmonics are damped and the perturbated region extends further. The generation of thermal harmonics near the ends of the stack will have an impact on heat transport between the stack and the heat-exchangers and it should be accounted for when optimizing the design of thermoacoustic systems.

Acknowledgments

The authors are grateful to Dr. Siva Mangalam from Tao Systems Inc who permitted the use of a CVA prototype, and to Emmanuel Jondeau for his help with the fabrication of the probes. They are also indebted to Prof. Vitalyi Gusev for his help with the model and to Paul Réglat who contributed to initial developments of this work.

References

[1] A. Berson, Ph. Blanc-Benon, Nonperiodicity of the flow within the gap of a thermoacoustic couple at high amplitudes, J. Acoust. Soc. Am. 122 (2007) EL122–EL127.
[2] A. Berson, Vers la miniaturisation des réfrigérateurs thermoacoustiques: Caractérisation du transport non-linéaire de chaleur et des écoulements secondaires, Ph.D dissertation (in French), Ecole Centrale de Lyon, ECL-2007-41 (2007).
[3] A. Berson, Ph. Blanc-Benon, "Nonlinear heat transport between the stack and the heat-exchangers of standing-wave thermoacoustic refrigerators", in: Proceedings of the 18th International Symposium on Nonlinear Acoustics, Stockholm, July 7–10, 2008, AIP Conference Proc. 1022, p. 359–362.
[4] A. Berson, Ph. Blanc-Benon, G. Comte-Bellot, A strategy to eliminate all nonlinear effects in constant-voltage anemometry, Rev. Sci. Instrum. 80 (2009) 045102.
[5] A. Berson, G. Poignand, Ph. Blanc-Benon, G. Comte-Bellot, Capture of instantaneous temperature in oscillating flows: use of constant-voltage anemometry to correct the thermal lag of cold wires operated by constant-current anemometry, Rev. Sci. Instrum. 81 (2010) 015102.
[6] A. Berson, Ph. Blanc-Benon, G. Comte-Bellot, On the use of hot-wire anemometry in pulsating flows. A comment on 'A critical review on advanced velocity measurement techniques in pulsating flows', Meas. Sci. Tech. 21 (12) (2010) 128001.
[7] E. Besnoin, O. Knio, Numerical study of thermoacoustic heat exchangers, Acta Acustica united with Acustica 90 (2004) 432–444.
[8] P. Freymuth, Velocity-induced harmonics for the thin-wire resistance thermometer, J. Phys. E: Sci Instrum. 12 (1979) 351–352.
[9] V. Gusev, P. Lotton, H. Bailliet, S. Job, M. Bruneau, Relaxation-time approximation for analytical evaluation of temperature field in thermoacoustic stack, J. Sound Vibr. 235 (2000) 711–726.
[10] V. Gusev, P. Lotton, H. Bailliet, S. Job, M. Bruneau, Thermal wave harmonics generation in the hydrodynamical heat transport in thermoacoustics, J. Acoust. Soc. Am. 109 (2001) 84–90.
[11] G. Huelsz, E. Ramos, Temperature measurements inside the oscillatory boundary layer produced by acoustic waves, J. Acoust. Soc. Am. 103 (1998) 1532–1537.
[12] S. Karpov, A. Prosperetti, A nonlinear model of thermoacoustic devices, J. Acoust. Soc. Am. 112 (2002) 1431–1444.
[13] J. Liu, S.L. Garrett, Relationship between Nusselt number and the thermoviscous (Rott) functions, J. Acoust. Soc. Am. 119 (2006) 1457–1462.
[14] D. Marx, Ph. Blanc-Benon, Numerical simulation of stack-heat exchangers coupling in a thermoacoustic refrigerator, AIAA J. 42 (7) (2004) 1338–1347.
[15] D. Marx, Ph. Blanc-Benon, Computation of the temperature distortion in the stack of a standing-wave thermoacoustic refrigerator, J. Acoust. Soc. Am. 118 (2005) 2993–2999.
[16] K.I. Matveev, G.W. Swift, S. Backhaus, Temperatures near the interface between an ideal heat exchanger and a thermal buffer tube or pulse tube, Int. J. Heat Mass Transfer 49 (2006) 868–878.
[17] K.I. Matveev, G.W. Swift, S. Backhaus, Analytical solution for temperature profiles at the ends of thermal buffer tubes, Int. J. Heat Mass Transfer 50 (2007) 897–901.
[18] G. Mozurkewich, Heat transfer from transverse tubes adjacent to a thermoacoustic stack, J. Acoust. Soc. Am. 110 (2001) 841–847.
[19] G.R. Sarma, Transfer function analysis of the constant voltage anemometer, Rev. Sci. Instrum. 69 (1998) 2385–2391.
[20] G.R. Sarma, R.W. Lankes, Automated constant voltage anemometer with in situ measurements of overheat and time constant of the hot wire, Rev. Sci. Instrum. 70 (1999) 2384–2386.
[21] L. Shi, X. Mao, A.J. Jaworski, Application of planar laser induced fluorescence measurement techniques to study heat transfer characteristics of parallel-plate heat exchangers in thermoacoustic devices, Meas. Sci. Technol. 21 (11) (2010) 115405.
[22] G.W. Swift, Thermoacoustic engines, J. Acoust. Soc. Am. 84 (1988) 1145–1180.
[23] M. Wetzel, C. Herman, Experimental study of thermoacoustic effect on a single plate part I: Temperature fields, Heat Mass Transf. 36 (2000) 7–20.